

The authors made a genuine effort in responding to the reviewers concerns and overall most of the issues have been adequately addressed. However, I am surprised how little of the response material has been included into the revised manuscript. Reviewers typically raise questions/comments not for themselves, but rather from the readers perspective. I recommend that a lot more of the response material would be included into the revised manuscript. For example, the response on the neutralization degree can briefly be mentioned in the text and the Figure included into Supplementary Material; discussion on validation of the proposed method by carbon isotope analysis did not make into revised manuscript; and so on.

**Response:**

We again appreciate the reviewer's further comments. We have added more discussions in the final version of the paper based on this recommendation, such as including the discussion on the neutralization degree, and the method of calculating mass concentrations of ammonia sulfate and ammonia nitrate (Lines 239–241). The corresponding Figure has also been added in the supplemental document (Fig. S3).

The carbon isotope analysis is a good method to identify the source of BC; however, as mentioned in our previous response to the referees, this method was usually used to distinguish the fossil-fuel combustion and biomass burning produced BC. It is difficult to distinguish the traffic-related BC from other fossil-fuel combustion sources, e.g., coal combustion. Thus, we only briefly compared our result to that based on carbon isotope analysis in the revised manuscript (Lines 409–411).

Response on defining thickly coated particles makes sense now and I suggest to look at the rBC size of the thinly coated particles. This presents some sort of validation (the major deficiency of the paper) where traffic related rBC core size derived from regression should roughly match the core size of thinly coated particles. Considering urban Beijing area having no major industrial sources, traffic related particles should stay thinly or non coated due to a short residence time after being emitted. Two peaks in lag time suggest two distinct populations with the traffic related particles clustering around short lag time while traffic related particles from long ranges and produced by

biomass burning possessing larger lags (the more severe pollution the larger the percentage of thickly coated particles). Therefore, while the regression may indeed point correctly at traffic related rBC cores having VED of 150nm, similar VED should be revealed by thinly coated particles which should arise from nearby traffic sources. My question is what is the rBC VED of the particles having a lag of approximately 1 $\mu$ s and 0 $\mu$ s? If the above question is positively responded it would significantly strengthen the paper.

Response:

We greatly appreciate the reviewer for providing this constructive comment, which provided us an idea for strengthening the paper. Accordingly, we calculated the VED of non/thinly coated rBC (lag time shorter than 2  $\mu$ s) with 5-min resolution and presented its frequency histogram in Fig. S4 as a supplemental material (also shown below). The frequency histogram can be well fitted by a Gauss function with the peak diameter of 149.2 nm. The value is almost the same as the mean of the entire 5-min VEDs of non/thinly coated rBC (149.5 nm). Both the peak diameter of gauss fitting and the mean diameter are close to the deductive VED of rBC from local traffic source (~150 nm) discussed in our manuscript. Such a finding further proves our hypothesis and conclusions already discussed in the paper, since the non/thinly coated rBC particles in urban Beijing are likely most from the local traffic exhausts. We have added a brief discussion based on this finding in the final version of the paper (Lines 329–334).

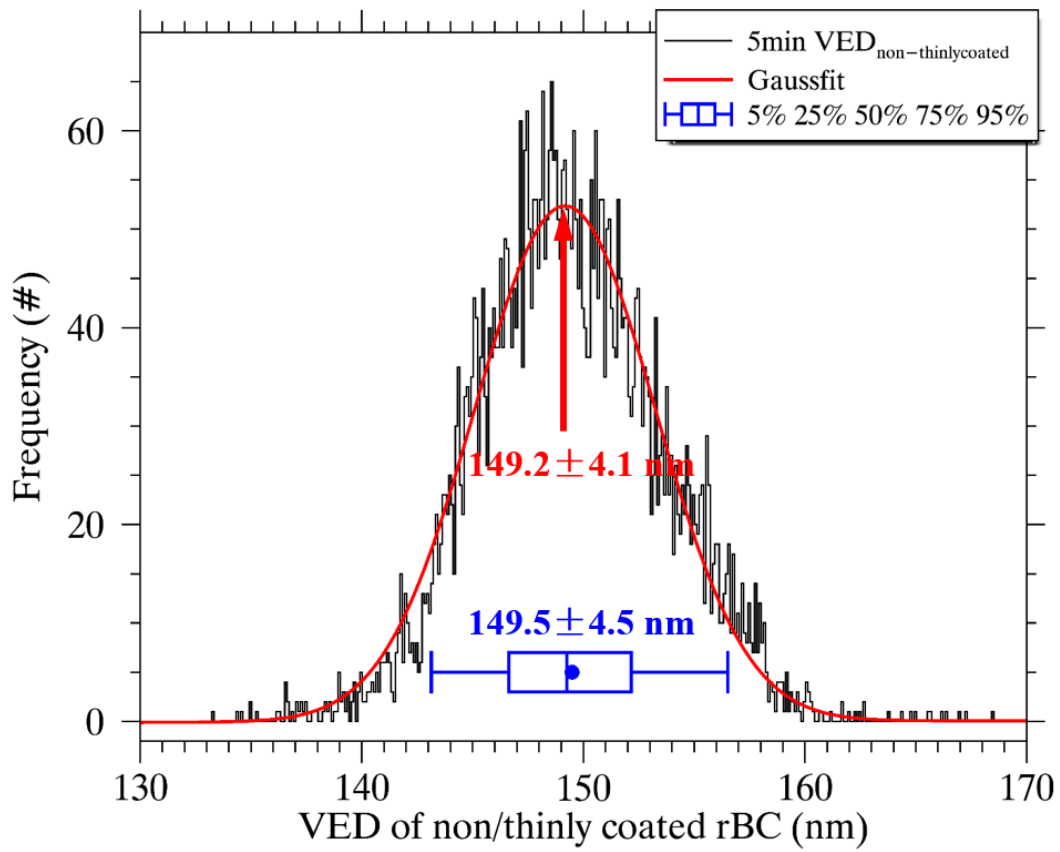


**Fig. S4.** Frequency histogram of the 5-min average volume-equivalent diameters (*VED*) of rBC without or with thin coating (black line). Gauss fitting is performed to the histogram (red line). Boxplot of the *VED* of non/thinly coated rBC is also overlapped (blue box).

1 **Marked-up manuscript version**

2 **Size distribution and source of black carbon aerosol in**  
3 **urban Beijing during winter haze episodes**

4 Yunfei Wu<sup>1,\*</sup>, Xiaojia Wang<sup>1</sup>, Jun Tao<sup>2</sup>, Rujin Huang<sup>3</sup>, Ping Tian<sup>4</sup>, Junji Cao<sup>3</sup>, Leiming  
5 Zhang<sup>5</sup>, Kin-Fai Ho<sup>6</sup>, Zhiwei Han<sup>1</sup>, Renjian Zhang<sup>1,\*</sup>

6  
7 1 CAS Key Laboratory of Regional Climate-Environment for Temperate East Asia,  
8 Institute of Atmospheric Physics, Chinese Academy of Sciences, Beijing, China

9 2 South China Institute of Environmental Sciences, Ministry of Environmental  
10 Protection, Guangzhou, China

11 3 CAS Key Laboratory of Aerosol Chemistry and Physics, Institute of Earth  
12 Environment, Chinese Academy of Sciences, Xi'an, China

13 4 Beijing Weather Modification Office, Beijing, China

14 5 Air Quality Research Division, Science and Technology Branch, Environment and  
15 Climate Change Canada, Toronto, Canada

16 6 The Jockey Club School of Public Health and Primary Care, The Chinese  
17 University of Hong Kong, Hong Kong, China

18

19 \* Correspondence to: Yunfei Wu (wuyf@mail.iap.ac.cn) and Renjian Zhang (zrj@mail.iap.ac.cn)

20

21 **Abstract**

22 Black carbon (BC) has important impact on climate and environment due to its  
23 light absorption ability, which greatly depends on its physicochemical properties  
24 including morphology, size and mixing state. The size distribution of the refractory  
25 BC (rBC) was investigated in urban Beijing during the late winter of 2014 with  
26 frequent haze events through analysis of measurements obtained using a single  
27 particle soot photometer (SP2). By assuming void-free rBC with a density of 1.8 g  
28 cm<sup>-3</sup>, the mass of the rBC showed an approximately lognormal distribution as a  
29 function of the volume-equivalent diameter (*VED*), with a peak diameter of 213 nm.  
30 Larger *VED* values of the rBC were observed during polluted periods than clean days,  
31 implying an alteration in the rBC sources, as the size distribution of the rBC from a  
32 certain source was relatively stable and *VED* of an individual rBC varied little once it  
33 was emitted into the atmosphere. The potential source contribution function analysis  
34 showed that air masses from the south to east of the observation site brought higher  
35 rBC loadings with more thick coatings and larger core sizes. The mean *VED* of the  
36 rBC presented a significant linear correlation with the number fraction of thickly  
37 coated rBC, extrapolating to be ~150 nm for the completely thinly/non coated rBC. It  
38 was considered as the typical mean *VED* of the rBC from local traffic sources in this  
39 study. Local traffic was estimated to contribute 35% to 100% of the hourly rBC mass  
40 concentration with a mean of 59% during the campaign. Lower local traffic  
41 contributions were observed during polluted periods, suggesting increasing  
42 contributions of other sources (e.g., coal combustion/biomass burning) to the rBC.  
43 Thus, the heavy pollution in Beijing was greatly influenced by other sources in  
44 addition to the local traffic.

45 **Keywords:** black carbon aerosol, size distribution, source, haze

46

## 47 **1 Introduction**

48 Black carbon (BC), the major light-absorbing chemical component in  
49 atmospheric aerosols, plays an important role in the radiative balance of the earth  
50 system through its direct effect of heating the lower atmosphere and indirect effect of  
51 affecting cloud properties (Ramanathan and Carmichael, 2008). Although BC is  
52 hydrophobic, it can still act as cloud condensation nucleus when internally mixed with  
53 hydrophilic chemical compounds (Zhang et al., 2008a), and thus indirectly affect  
54 cloud properties and associated radiative budget (Ramanathan et al., 2001). BC  
55 aerosols thus have great impacts on regional and global climate and weather (Menon  
56 et al., 2002; Ramanathan and Carmichael, 2008; Ding et al., 2013; Liao et al., 2015;  
57 Huang et al., 2016). BC can also increase atmospheric stability through its heating  
58 effect in the lower troposphere and cooling role at the surface (Wang et al., 2013),  
59 which in turn suppresses the diffusion of pollutants, deteriorates air quality, and  
60 enhances haze weather intensity (Ding et al., 2016). However, quantifying BC's  
61 impact on radiative forcing and environment is challenging and has large uncertainties  
62 because of the large variations in its concentration and physicochemical properties  
63 (IPCC, 2013). The light absorption of BC highly depends on its size distribution and  
64 morphology. Mie calculations for hypothetical BC spheres show that the mass  
65 absorption cross-sections reach their peaks at a diameter of ~150 nm and then  
66 decrease sharply with further increases in size (see Fig. 4 in Bond and Bergstrom,  
67 2006). However, atmospheric BC particles apparently consist of aggregates of small  
68 primary spherules ~15 to 60 nm in diameter (Alexander et al., 2008; Zhang et al.,  
69 2008a). They are chain agglomerates when freshly emitted from the combustion  
70 sources resulting in increasing mass normalized absorption with the particle mobility  
71 size (Khalizov et al., 2009). These fresh BC particles are quickly coated by other  
72 aerosol components in the atmosphere, leading to the collapse of the chain  
73 agglomerates into more compact BC cores (Zhang et al., 2008a). An alteration in the  
74 morphology of BC due to a thin coating causes competition between light absorption  
75 enhancement and decline, resulting in little variation in the absorption efficiency  
76 (Wang et al., 2013; Peng et al., 2016). Subsequently, the thickened coating of the

77 scattering shell enwrapping the compact BC cores enhances the light absorption of  
78 BC by the lensing effect, although the upper limit of the enhanced amplitude varied  
79 among different studies (e.g., Schnaiter et al., 2005; Shiraiwa et al., 2010; Khalizov et  
80 al., 2009; Peng et al., 2016).

81 With its rapid economic development, China has been suffering from heavy air  
82 pollution (Yin and Wang, 2016). Annual BC emissions to the atmosphere in China are  
83 very high, accounting for approximately half of the total emissions in Asia and  
84 one-fifth globally (Qin and Xie, 2012). Existing studies on ambient BC mostly  
85 focused on its mass concentrations (e.g., Cao et al., 2007; Zhang et al., 2008b), and  
86 little is known about its physicochemical properties, including size, morphology, and  
87 mixing state (e.g., Huang and Yu, 2008; Cheng et al., 2012), mainly due to the  
88 limitations of the measurement methodology. A traditional approach determining BC  
89 size distribution is through analyzing the BC mass of size-segregated aerosol samples  
90 (Huang and Yu, 2008; Yu et al., 2010), which provides size information of  
91 BC-containing particles because BC particles are frequently internally mixed with  
92 other aerosol components in the atmosphere (Shiraiwa et al., 2007; Schwarz et al.,  
93 2008). The time resolution in this approach was typically from hours to days. In the  
94 most recent decade, a novel analyzer, single particle soot photometer (SP2), has been  
95 developed, which can measure mass and size of the refractory BC (rBC) in high time  
96 resolution (Stephens et al., 2003; Schwarz et al., 2006). The mixing state of rBC  
97 particles can also be derived from the measurement of SP2 (Gao et al., 2007; Moteki  
98 and Kondo, 2007, 2008; Laborde et al., 2012). Measurements of the sizes and mixing  
99 states of rBC based on this technology has been limited to a few regions in China (e.g.,  
100 Huang et al., 2012; Wang et al., 2014a, 2015a; Wu et al., 2016; Gong et al., 2016), as  
101 the SP2 is very expensive and its performance is limited (Gysel et al., 2012; Liggio et  
102 al., 2012). It should be noted that the sizes of rBC reported by SP2 are generally  
103 mass-equivalent diameters rather than mobility- or aerodynamic-based ones, which  
104 are determined on the basis of the mass measurements of individual rBC-containing  
105 particles. Thus, they are independent of the morphology or mixing.

106 Although the physicochemical properties of BC in the atmosphere are greatly

107 diverse, its mass-equivalent sizes should vary little during their typical lifetime in the  
108 atmosphere (~1 week) since BC itself is chemically inert under ambient conditions. In  
109 other words, the mass-size of a BC particle is independent of its morphology and  
110 mixing state, although coating with other components will reduce its mobility  
111 diameter and enlarge the size of the mixed particle in which the BC is embedded. As  
112 it is a byproduct of the incomplete combustion of fossil fuels and biomass, the BC  
113 size should be highly dependent on the emission sources, including fuel type and  
114 combustion condition. Based on the measurement of SP2, Liu et al. (2014) showed  
115 smaller sizes of the rBC cores from traffic than those from solid fuel sources and  
116 attributed the rBC concentrations from the two dominant sources accordingly. The  
117 rBC sizes measured at rural or remote sites were considerably larger than those  
118 measured at urban sites (Huang et al., 2012; Schwarz et al., 2013), implying that  
119 smaller sizes of rBC are emitted from traffic sources. Combining the measurement of  
120 SP2 and the chemical source apportionment of daily PM<sub>2.5</sub> samples, Wang et al. (2016)  
121 showed that the rBC from biomass burning and coal combustion had larger  
122 mass-equivalent diameter than that from traffic.

123 Influenced by the local emissions (e.g., traffic exhaust) as well as regional  
124 transport of air pollutants from the surrounding heavily polluted areas, the  
125 physicochemical properties of ambient BC aerosols in urban Beijing varied greatly. In  
126 this study, the mass-equivalent size distributions of rBC were first revealed in urban  
127 Beijing based on the SP2 measurement during a wintertime in 2014 when haze  
128 occurred frequently. The variations in the rBC size were also investigated,  
129 accompanied by an analysis of their relationships with aerosol chemical composition  
130 and rBC's potential source contributions. In the present study, a novel approach was  
131 employed to evaluate the contribution of local traffic to the rBC concentration based  
132 on the measured rBC sizes and reasonable assumptions including a deductive mean  
133 diameter of rBC from local traffic and relatively stable rBC sizes in the air masses  
134 transported over certain regions.

135

## 136 **2 Methodology**



137 In situ measurements of rBC were conducted using a SP2 (Droplet Measurement  
138 Technology, Inc., Boulder, CO, USA) on the rooftop (approximately 8 m above  
139 ground level) of an experimental building at the Tower Division of the Institute of  
140 Atmospheric Physics, Chinese Academy of Sciences (39°58'N, 116°22'E), during a  
141 late winter period from 24 February to 15 March 2014 before the residential heating  
142 season ended. The SP2 directly detects the incandescent intensity of an individual  
143 rBC-containing particle when it passes through an intra-cavity Nd:YAG laser beam  
144 with a Gaussian distribution (Schwarz et al., 2006). The incandescent intensity is  
145 converted to the mass of rBC based on the calibration of incandescent signals of  
146 size-selected soot standards performed pre/post-sampling. In this study, the Aquadag  
147 (Acheson, Inc., USA) was used as a reference rBC and size-selected by a scanning  
148 mobility particle sizer spectrometer (SMPS; TSI, Inc., Shoreview, MN, USA) for  
149 calibration. Compared to the ambient rBC, it is more sensitive to the incandescence  
150 signal. Thus, a scaling factor of 0.75 is employed with the calibration curve to induce  
151 more reliable rBC mass determinations (Baumgardner et al., 2012; Laborde et al.,  
152 2012). Moreover, an approximately 10% underestimation of the SP2-derived bulk  
153 rBC mass concentration due to the detection limitations outside the rBC mass range of  
154 ~0.3–120 fg was considered (Wang et al., 2014a, 2015a). The total uncertainty in the  
155 rBC mass determination was ~25%, including the uncertainties inherent in the mass  
156 calibration, flow measurement and estimation of BC masses beyond the SP2 detection  
157 range (Wu et al., 2016). The scattering signal is synchronously detected by the SP2  
158 and used to determine the optical size of a single particle (Gao et al., 2007; Laborde et  
159 al., 2012). In this study, the scattering signal was employed to distinguish the mixing  
160 state of rBC-containing particles. A traditional method based on the delay time  
161 between the incandescent and scattering peaks was utilized to distinguish the rBC  
162 cores with and without a thick coating (Schwarz et al., 2006; Moteki and Kondo, 2007;  
163 Wang et al., 2014a; Wu et al., 2016). The rBC-containing particles were defined as  
164 either thickly coated or uncoated/thinly coated according to the distribution of  
165 detected lag times, which was bimodal and had a local minimum at 2  $\mu$ s (Fig. S1 in  
166 the supplemental files). We defined the rBC particles as thickly coated if the lag times

167 were longer than 2  $\mu\text{s}$ . On this basis, the number fraction of thickly coated rBC  
168 ( $NF_{\text{coated}}$ ), defined as the ratio of the number of thickly-coated rBC particles to that of  
169 all detectable rBC particles, was calculated to characterize the relative mixing extent  
170 of the BC aerosols in different ambient samples. A similar measurement was  
171 conducted in January 2013, and more details of the experimental setup and data  
172 process can be found in Wu et al. (2016).

173 Samples of  $\text{PM}_{2.5}$  were collected twice a day during this campaign, each lasting  
174 for twelve hours. The chemical contents including organic carbon (OC), elemental  
175 carbon (EC), water-soluble ions (e.g.,  $\text{SO}_4^{2-}$ ,  $\text{NO}_3^-$ , and  $\text{NH}_4^+$ ) and trace elements  
176 were analyzed in the laboratory, as presented in detail by Lin et al. (2016).

177

### 178 **3 Results and Discussion**

#### 179 **3.1 Size distribution of rBC and its variation**

180 As shown in Fig. 1, the mass of rBC ( $dM/d\log D_p$ ) exhibited an approximately  
181 lognormal distribution as a function of the volume-equivalent diameter ( $VED$ ) of  
182 void-free rBC, as has been commonly observed (e.g., Schwarz et al., 2006; Huang et  
183 al., 2012; Wang et al., 2016). The similar size distribution was also observed in our  
184 previous campaign in January 2013 (Fig. S2 in the supplemental files). A minor mode  
185 was also captured at large sizes (peaked at  $\sim 600$  nm), only accounting for  $\sim 6\%$  of the  
186 SP2-determined rBC masses. An analogous minor mode was previously observed at  
187 other sites in China. Huang et al. (2011) reported a minor peak with a diameter of  
188  $\sim 690$  nm at Kaiping, a rural site in the Pearl River Delta (PRD) region of China. Wang  
189 et al. (2014b) found a minor peak with a diameter of  $\sim 470$ – $500$  nm in a remote area of  
190 the Qinghai–Tibetan Plateau and considered it a likely feature of the rBC distribution  
191 of biofuel/open fire burning sources, which needs further verification using  
192 measurements of the size distributions at the emission sources. The peak diameter of  
193 the primary mode, with a value of 213 nm, during the campaign is well within the  
194 range ( $\sim 150$ – $230$  nm) presented by previous studies conducted in different regions  
195 (Huang et al., 2012 and references therein). It should be noted that the density of the  
196 assumed void-free rBC was set to be  $1.8 \text{ g cm}^{-3}$  in calculating the  $VED$  from the rBC

197 masses measured in this study, which should result in larger *VED* values compared to  
198 those based on the density of  $2.0 \text{ g cm}^{-3}$  used in previous studies. If the density of  $2.0$   
199  $\text{g cm}^{-3}$  was employed, the peak diameter of the primary mode would be  $\sim 206 \text{ nm}$  in  
200 this study. This value is very close to those observed in urban areas throughout China,  
201 e.g.,  $210 \text{ nm}$  in Shenzhen in South China (Huang et al., 2012),  $205 \text{ nm}$  in Xi'an in  
202 West China (Wang et al., 2015b), and  $\sim 200 \text{ nm}$  in Shanghai in East China (Gong et al.,  
203 2016). The relatively similar mass-size distributions of rBC suggest that there were  
204 similar dominant emission sources in different urban regions in China, where vehicle  
205 exhaust was one of the important sources emitting rBC particles. Compared to those  
206 measured at rural sites in the PRD region in South China (e.g.,  $220\text{--}222 \text{ nm}$ , Huang et  
207 al., 2011, 2012), the peak diameters of rBC in urban areas are significantly smaller.  
208 This might be related to the greater amounts of coal combustion and biomass burning  
209 around the rural sites (Huang et al., 2012). In contrast, the sizes of the rBC were much  
210 smaller in remote regions, e.g., with a peak diameter of  $\sim 175\text{--}188 \text{ nm}$  in the Qinghai–  
211 Tibetan Plateau area (Wang et al., 2014b, 2015a). Wang et al. (2015a) attributed this  
212 smaller peak diameter value to the source and considered that biomass burning  
213 generated a small rBC with peak *VED* values in the range of  $\sim 187\text{--}193 \text{ nm}$ . Another  
214 important reason for the smaller rBC measured in remote regions, in our opinion, is  
215 that more large rBC particles are deposited during their long-range transport to the  
216 observation site. Further research on the sizes of rBC from different sources is  
217 needed.

218 The mass-size distributions of rBC during a polluted day (25 February) and a  
219 clean one (4 March) are also compared in Fig. 1. The average mass concentrations of  
220 rBC ( $MC_{\text{rBC}}$ ) were  $7.6 \mu\text{g m}^{-3}$  and  $0.4 \mu\text{g m}^{-3}$ , respectively, on the polluted and clean  
221 days. The size distribution of rBC during the polluted day is similar to that during the  
222 entire observation period, although a larger peak diameter was observed, with a value  
223 of  $221 \text{ nm}$ . In contrast, the peak diameter on the clean day is obviously smaller, with a  
224 value of  $199 \text{ nm}$ . The secondary mode cannot be well characterized on the clean day.  
225 As mentioned above, the mass-sizes of rBC emitted from a certain source change little  
226 during their lifetime in the atmosphere. Thus, the considerable discrepancy of the rBC

227 sizes illustrates significant source alteration during the polluted period compared to  
228 that on a clean day. Sun et al. (2014) used the measurements of ACSM at an urban  
229 site in Beijing to show that the regional contribution to the BC exceeded 50% during  
230 heavily polluted periods in January 2013. Model simulation also revealed that  
231 regional transport contributed an average of 56% to the  $PM_{2.5}$  in Beijing in January  
232 2013 when the hazes occurred frequently, and even higher during polluted periods (Li  
233 and Han, 2016). Accordingly, regional transport might play an important role in the  
234 increase in rBC sizes during polluted periods in urban Beijing. By comparison, traffic  
235 emissions should be the dominant source of rBC on the clean day, contributing to  
236 smaller rBC sizes.

237 The variation in the  $VED$  of the rBC is further investigated by comparing the  
238 mean  $VED$  value of rBC ( $VED_{rBC}$ ) with the mass ratios of secondary inorganic  
239 components (i.e., ammonium sulfate, AS; ammonium nitrite, AN) to EC, a  
240 representation of the aerosol aging degree. Note that AS mass was calculated as 1.375  
241 times of sulfate mass and AN mass as 1.29 times of nitrate mass because the aerosol  
242 samples were almost neutral in ionic equilibrium (Fig. S3). Generally, the average  
243  $VED_{rBC}$  positively correlated with AS/EC and AN/EC ratios with correlation  
244 coefficients of 0.63 ( $p < 0.01$ ) and 0.61 ( $p < 0.01$ ), respectively (Fig. 2a and 2b). Higher  
245 AS/EC and AN/EC ratios were observed in polluted samples, corresponding to higher  
246  $VED_{rBC}$  during these periods.

247 It is interesting to note that the  $VED_{rBC}$  correlated more closely with AS/EC ratio  
248 than AN/EC, especially under a clean condition. The correlation coefficient between  
249  $VED_{rBC}$  and AS/EC is 0.88 ( $p < 0.01$ ) during clean periods with  $PM_{2.5}$  mass  
250 concentrations lower than  $35 \mu g m^{-3}$  (blue dots in Fig. 2), much higher than that  
251 between  $VED_{rBC}$  and AN/EC. By contrast, the  $NF_{coated}$  varied less with AS/EC during  
252 these periods (Fig. 2c). This means that a higher AS/EC had less effect on the fraction  
253 of thickly coated rBC during these clean periods but was related to larger rBC sizes,  
254 which were highly dependent on the emission sources. In other words, higher AS/EC  
255 values might indicate an increasing contribution of sources producing larger rBC  
256 other than traffic, as sulfur is one of the major pollutants of coal combustion but not

257 of traffic (Zhang et al., 2013; Wang et al., 2016). On the other hand,  $NF_{\text{coated}}$  was  
258 highly related to AN/EC, with a correlation coefficient of 0.81 ( $p < 0.01$ ) during the  
259 clean periods (Fig. 2d). Even considering the entire samples, the correlation  
260 coefficient between  $NF_{\text{coated}}$  and AN/EC was as high as 0.81 ( $p < 0.01$ ), much higher  
261 than that (0.65,  $p < 0.01$ ) between  $NF_{\text{coated}}$  and AS/EC. This implies that the mixing  
262 state of rBC is very sensitive to AN/EC in urban Beijing, especially during the clean  
263 periods. The secondary formation of AN might play an important role in the coating  
264 processes of rBC but has a negligible effect on the core size of the rBC.

265

### 266 **3.2 Potential source contribution to rBC mass and size**

267 The potential source contribution function (PSCF) analysis based on hourly  
268 resolved 48-h backward trajectories arriving at the observation site 100 m above  
269 ground level was performed using TrajStat software (Wang et al., 2009). The  
270 threshold of the PSCF analysis was set to the mean value of each variable. A weight  
271 function on the gridded PSCF values was employed on those cells having few  
272 trajectory endpoints (Wang et al., 2006). Generally, the areas east and south of the  
273 observation site had the largest number of potential source regions of high rBC  
274 concentrations, with weighted PSCF (WPSCF) values of  $MC_{\text{rBC}}$  larger than 0.7 (Fig.  
275 3a). Previous studies showed that Hebei province, on the southern and eastern borders  
276 of Beijing, was a major contributor to pollutants in Beijing, as its industrial activities  
277 are intense (Zhang et al., 2013). The high coal consumption associated with the heavy  
278 industrial activities and residential heating in the cold season should be an important  
279 source of high atmospheric rBC loading in these areas. Similarly, the distribution of  
280 the WPSCF values of  $VED_{\text{rBC}}$  shows that the eastern and southern regions are also  
281 correlated with large  $VED_{\text{rBC}}$  values (Fig. 3b). This implies that the pollution sources  
282 in these regions, e.g. heavy industrial activities and residential heating, tend to  
283 produce highly concentrated rBC-containing particles with large rBC core sizes. The  
284 source apportionment of rBC aerosols in London based on in situ SP2 measurements  
285 showed that rBC-containing particles from solid fuel sources (coal combustion and  
286 biomass burning) had significantly larger rBC cores than those from traffic (Liu et al.,

287 2014). Thus, the high WPSCF values of  $MC_{rBC}$  and  $VED_{rBC}$  in the east and south  
288 might highly correlate to anthropogenic coal/biomass combustion in these regions.

289 The spatial distribution of the WPSCF values of  $NF_{coated}$  is shown in Fig. 3c.  
290 Associated with the aging processes that increase the thickly coating states of  
291 rBC-containing particles through heterogeneous reactions, the WPSCF values of  
292  $NF_{coated}$  are generally high in the areas surrounding the observation site. It should be  
293 noted that higher WPSCF values of  $NF_{coated}$  ( $> 0.7$ ) dominate in the east to south. In  
294 addition to the transport of thickly coated BC particles from these regions, aging  
295 processes of locally emitted BC particles (e.g., from traffic sources) under the  
296 southerly winds dominant condition, in which the relative humidity (RH) is high  
297 (Zhang et al., 2015; Zheng et al., 2015), also increase the fraction of thickly coated  
298 rBC (Wu et al., 2016). Although northerly/northwesterly winds also blow aged  
299 rBC-containing particles with thick coatings, the larger amounts of non-/thinly coated  
300 BC particles from local sources during these periods diminished the WPSCF values of  
301  $NF_{coated}$  in the north to west regions of the observation site. The low RH and strong  
302 winds from these directions are unfavorable to the coating processes of locally  
303 emitted fresh rBC particles.

304 The  $VED_{coated}$ , defined as the  $VED$  of those thickly coated rBC cores, shows a  
305 dispersive WPSCF distribution (Fig. 3d). Compared to the distribution of  $VED_{rBC}$   
306 with high WPSCF values that dominate in the east to south, high WPSCF values of  
307  $VED_{coated}$  are located in the northern pathway of air masses being transported to the  
308 observation site as well. This implies that the regional transport of air masses brings  
309 large rBC, no matter which direction it comes from. Dominated by the locally emitted  
310 small rBC, the WPSCF values of  $VED_{rBC}$  are low in the northern region. It further  
311 illustrates that local sources such as traffic emit small rBC, while regional transport  
312 brings in large rBC. On the basis of the large discrepancy in rBC sizes between local  
313 traffic and regional transport generated particles, it is possible to extract the  
314 contribution of local traffic emissions from the mixed rBC sources.

315

#### 316 **4 Discussion**

#### 317 **4.1 Relationship between rBC size and mixing state**

318 As large rBC sizes are usually accompanied by significant contributions of  
319 regional transport, which also lead to a high fraction of thickly coated rBC, the  
320  $VED_{\text{rBC}}$  is directly compared with the  $NF_{\text{coated}}$  as shown in Fig. 4. The  
321 two-dimensional histogram of the 5-min average  $VED_{\text{rBC}}$  and  $NF_{\text{coated}}$  presents a  
322 significant linear correlation between the two variables. It is characterized more  
323 clearly by the variation in the mean  $VED_{\text{rBC}}$  values averaged in increased  $NF_{\text{coated}}$  bins  
324 with a resolution of 2% (magenta circles in Fig. 4). The observed minimum value of  
325 the 5-min  $NF_{\text{coated}}$  is ~10%, representing that there is little pure external mixing of  
326 rBC in the atmosphere, even for short periods. However, an assumed mean  $VED$  of  
327 completely non/thinly coated rBC is extrapolated from the linear curve to  $NF_{\text{coated}}$   
328 with a value of 0% (i.e., the y-intercept value). This inferred  $VED$ , with a value of  
329 ~150 nm, might be considered as the typical mean  $VED$  of freshly emitted rBC from  
330 vehicle exhaust, which has little coating (Zhang et al., 2008a; Peng et al., 2016). **This**  
331 **value is almost the same as the mean  $VED$  of observed rBC without or with thin**  
332 **coating (149.5±4.5 nm, Fig. S4 in the supplemental file). Since these non/thinly**  
333 **coated rBC are mostly from local traffic source in urban Beijing, knowing that local**  
334 **major industrial sources are very limited, the consistency in the inferred and mean**  
335  **$VED$  of non/thinly coated rBC verifies our hypothesis above.** It is surprising to find  
336 that the linear relationship between  $VED_{\text{rBC}}$  and  $NF_{\text{coated}}$  seems to be common, as was  
337 also found in another campaign conducted in January 2013 (Wu et al., 2016) (gray  
338 circles in Fig. 4). More observations are needed to further verify this relationship.  
339 According to the results presented in this study, a mean  $VED$  of ~150 nm is  
340 legitimately accepted as the typical SP2-determined mean  $VED$  of fresh rBC from  
341 local traffic sources. Size-segregated aerosol samples also revealed a mode peaked at  
342 ~150 nm in aerodynamic diameter for elemental carbon (EC) in urban Guangzhou, a  
343 megacity in PRD region, which were also attributed to traffic emissions (Yu and Yu,  
344 2009; Yu et al., 2010). A second mode at a diameter of ~400 nm was also observed  
345 and was also thought to be associated with traffic emission (Yu and Yu, 2009). In  
346 contrast, only the smaller EC mode with peak diameter in the range of 100–200 nm

347 was observed from traffic sources in urban areas of developed countries (Allen et al.,  
348 2001; Kleeman et al., 2000). To date, no literature is available for comparison with the  
349 case in Beijing because of the limitation in characterizing the size distribution of EC  
350 at the small mode (e.g., < 400 nm). Considering the stringent fuel and vehicle  
351 emission standards implemented in Beijing, the *VED* of ~150 nm for local traffic  
352 source is reasonable, although further measurement studies are still needed to verify  
353 this. As mentioned above, the *VED* of certain rBC varies little once it is emitted to the  
354 atmosphere. Thus, the mean *VED* with a value of ~150 nm was employed in this study  
355 as the representative of the rBC size from local traffic.

356 The variation in  $VED_{\text{coated}}$  with  $NF_{\text{coated}}$  is also shown (magenta triangles in Fig.  
357 4). It is interesting to find that, compared to  $VED_{\text{rBC}}$ ,  $VED_{\text{coated}}$  presents a fluctuant  
358 variation as  $NF_{\text{coated}}$  increases. The larger  $VED_{\text{coated}}$  at lower  $NF_{\text{coated}}$  is comprehensible  
359 because regionally transported large rBC dominates in the thickly coated rBC  
360 particles, and the small rBC from local traffic is mainly externally mixed with other  
361 aerosol components at this stage. As the  $NF_{\text{coated}}$  increases from 10–20% to 30–40%,  
362 the mean  $VED_{\text{coated}}$  gradually decreases from ~200 nm to ~190 nm. This implies that  
363 some small rBC (e.g., rBC from local traffic) contributes a considerable portion of the  
364 thickly coated rBC particles at this stage. In addition to the influence of the emission  
365 sources on the rBC size, this decrease in  $VED_{\text{coated}}$  can also be explained by the  
366 contamination of the local traffic emitted small rBC into the thickly coated rBC  
367 particles through atmospheric aging processes (i.e., coating with other components). It  
368 should be noted that the  $VED_{\text{rBC}}$  sustained increases at this stage, implying that other  
369 sources besides the local traffic also brought large rBC at the same time. This is  
370 because if the increase in  $NF_{\text{coated}}$  only results from the coating processes of the local  
371 traffic emitted rBC, the *VED* of the entire rBC (i.e.,  $VED_{\text{rBC}}$ ) should vary little. The  
372  $VED_{\text{coated}}$  increases significantly when  $NF_{\text{coated}}$  exceeds 40%, suggesting that regional  
373 transport dominates at this stage, bringing in a large amount of thickly coated rBC  
374 particles with a large rBC core. Meanwhile, the mean  $MC_{\text{rBC}}$  increases dramatically  
375 from  $1.3 \mu\text{g m}^{-3}$  to  $5.0 \mu\text{g m}^{-3}$  when  $NF_{\text{coated}}$  increases from 30% to 50%, further  
376 confirming the great contribution of regional transport to the rBC at this stage. By



377 comparison, the mean rBC concentration varies in a small range of 0.8–1.4  $\mu\text{g m}^{-3}$   
378 when  $NF_{\text{coated}}$  is lower than 30%. The observation from the campaign of 2013 showed  
379 a similar variation in  $VED_{\text{coated}}$  against  $NF_{\text{coated}}$  (gray triangles in Fig. 4).

380

#### 381 **4.2 Extracting the local traffic contribution to rBC**

382 As  $VED_{\text{rBC}}$  with a value of  $\sim 150$  nm is expected to be the typical mean  $VED$  of  
383 the local traffic emitted rBC and varies little in the atmosphere, it provides the  
384 possibility of extracting the contribution of the local traffic to the rBC from the total  
385 rBC mass concentration according to the variation in  $VED_{\text{rBC}}$ . However, the typical  
386 mean  $VED$  of rBC from other sources, such as coal combustion and biomass burning,  
387 is difficult to identify. It depends on many factors including fuel type and combustion  
388 condition. In this study, a simple assumption was employed to identify the typical  
389 mean  $VED$  of rBC from other sources besides local traffic according to where the air  
390 masses came from. During a short period when the source emissions were relatively  
391 stable, the rBC from a certain direction was assumed to have a certain mean  $VED$ , no  
392 matter from which source it is emitted. Thus, a cluster analysis was performed on the  
393 48-h backward trajectories that arrived at the observation site. Five clusters were  
394 identified using TrajStat software according to the total spatial variation in the cluster  
395 numbers (as shown in Fig. S5). As the rBC tends to be thickly coated in the regionally  
396 transported air masses, the mean  $VED$  of the rBC from sources other than local traffic  
397 was derived from the values of  $VED_{\text{coated}}$ . The local traffic emitted small rBC can also  
398 become thickly coated through aging processes in the atmosphere, so a further  
399 assumption is employed to consider the  $VED$  of rBC from other sources equal to the  
400 mean value of the upper 5% percentile of  $VED_{\text{coated}}$  in each cluster. Five typical mean  
401  $VED$ s of rBC from sources other than local traffic were identified, with values in the  
402 range of 195.5–208.3 nm (Fig. S5). Such simple assumptions might induce large  
403 uncertainties in the absolute contribution of the local traffic to the rBC, but it should  
404 well reflect the variation in the traffic contribution.

405 Using a multiple linear regression to  $VED_{\text{rBC}}$ , the hourly-resolved traffic  
406 contribution to the rBC was extracted on the basis of the derived  $VED$  of the rBC

407 from local traffic and other sources. The mass fraction of the traffic-induced rBC  
408 ( $MF_{\text{traffic}}$ ) is shown in Fig. 5a (red line). During this campaign, approximately 35% to  
409 100% of the hourly  $MC_{\text{rBC}}$  is attributed to local traffic emissions, with a mean of 59%.  
410 Although carbon isotope analysis is commonly used in BC/EC source identification  
411 (Zhang et al., 2015; Liu et al., 2016), it is difficult to use this method to distinguish  
412 the traffic-related source from other fossil-fuel combustion sources. Based on a  
413 multiple linear regression analysis of the contributions of the three dominant factors  
414 (i.e., traffic, coal combustion and biomass burning) to the rBC derived from the  
415 chemical source apportionment of the daily  $PM_{2.5}$  samples, Wang et al. (2016) showed  
416 a slightly lower contribution of the traffic to the rBC in urban Xi'an, with a mean of  
417 46% and a daily contribution in the range of 0.8 to 77.2%. Since entirely different  
418 methods were employed in addition to the different locations, the resolved traffic  
419 contribution to the rBC should not be compared absolutely. However, the relatively  
420 lower  $MC_{\text{rBC}}$  in this study (with a mean of  $2.8 \mu\text{g m}^{-3}$  compared to  $8.0 \mu\text{g m}^{-3}$ ) might  
421 partly interpret the slightly higher contribution of traffic, as a lower  $MC_{\text{rBC}}$  is usually  
422 accompanied by a higher contribution of the local traffic. It is clear that  $MF_{\text{traffic}}$  is  
423 negatively correlated with  $MC_{\text{rBC}}$ , with the correlation coefficient as high as -0.84  
424 ( $p < 0.01$ ) between the daily moving averaged  $MF_{\text{traffic}}$  and  $MC_{\text{rBC}}$  (Fig. 5a). This means  
425 that the traffic contribution to the rBC decreased significantly during the polluted  
426 periods when the rBC loading increased. In other words, the rBC from other sources  
427 such as coal combustion and biomass burning played an increasing role in these  
428 polluted periods. This implies that the high  $MC_{\text{rBC}}$  in urban Beijing was not only due  
429 to the accumulation of the local traffic emissions during stable synoptic conditions but  
430 also attributed to the overlaying pollution from other sources.

431 The diurnal variations of the decomposed  $MC_{\text{rBC}}$  from local traffic and other  
432 sources are shown in Fig. 5b and 5c, respectively. A common diurnal variation in  
433  $MC_{\text{rBC}}$  with higher values during the nighttime and lower ones in the daytime is  
434 shown for both the traffic and other sources produced rBC, suggesting the important  
435 impact of the mixing layer height on the surface  $MC_{\text{rBC}}$ . A high mixing layer in the  
436 daytime, especially in the afternoon, favors the diffusion of the pollutants, leading to a

437 low value of  $MC_{\text{rBC}}$ . A low mixing layer in the nighttime suppresses the diffusion of  
438 pollutants, resulting in a high value of  $MC_{\text{rBC}}$ . It is noted that a significant peak  $MC_{\text{rBC}}$   
439 of local traffic was observed in the early morning (05:00–06:00 local time). Moreover,  
440 the increase in the local traffic related  $MC_{\text{rBC}}$  occurs earlier than that of other sources  
441 in the evening. It corresponds well to the increased traffic contribution in the morning  
442 and evening rush hours. Although the traffic flow showed a significant decrease in the  
443 nighttime, a dramatic increase in the flow of heavy-duty diesel vehicles was observed  
444 due to traffic regulations in Beijing (Song et al., 2013). These vehicles have much  
445 higher emission factors of BC (~15–30 times) than light-duty gasoline ones, and thus  
446 play a non-negligible role in the high  $MC_{\text{rBC}}$  values around midnight. Generally, the  
447 diurnal variation of  $MC_{\text{rBC}}$  verifies to some degree the rationality of the method  
448 employed in this study for distinguishing the contribution of the local traffic emission  
449 from that of other sources.

450

## 451 **5 Summary and Concluding Remarks**

452 An approximate lognormal size distribution of the rBC in volume-equivalent  
453 diameter was observed in urban Beijing during a polluted winter in 2014 based on  
454 measurements using a SP2. The peak diameter was 213 nm, assuming void-free rBC  
455 with a density of  $1.8 \text{ g cm}^{-3}$ , which is close to the values observed in other urban areas  
456 in China. The measured sizes of the rBC were considerably larger during the polluted  
457 period than clean period, implying a source variation of the rBC. The mean  $VED_{\text{rBC}}$   
458 positively correlated with the ratios of secondary inorganic aerosols (including AS  
459 and AN) to EC, especially the ratio of AS/EC under a clean condition. This implies  
460 that the rBC sizes are highly related to the emission sources because sulfur is one of  
461 the major pollutants in coal combustion, while little is emitted from traffic. By  
462 comparison, the mean  $NF_{\text{coated}}$  correlated more with AN/EC, implying the important  
463 effect of the secondary formation of nitrate on the rBC mixing state. The PSCF  
464 analysis showed that regional transport from the east to south of Beijing was a major  
465 source of high rBC loading in Beijing and accompanied by a large  $VED_{\text{rBC}}$  and high  
466  $NF_{\text{coated}}$ .

467 A significant positive correlation existed between  $VED_{\text{rBC}}$  and  $NF_{\text{coated}}$ , inferring  
468 the typical mean  $VED$  of the rBC from local traffic, with a value of 150 nm. Based on  
469 the inferred  $VED$  and other assumptions, local traffic was estimated to contribute 59%  
470 of the  $MC_{\text{rBC}}$  on campaign average in urban Beijing. However, its contribution  
471 decreased significantly in the polluted period compared to the clean period. A  
472 significant negative correlation is found between the daily moving average  $MC_{\text{rBC}}$  and  
473  $MF_{\text{traffic}}$  with a coefficient of -0.87. A similar diurnal variation in the decomposed  
474  $MC_{\text{rBC}}$  associated with local traffic and other sources was observed with high values  
475 in the nighttime and low ones in the daytime. However, a significant increase in traffic  
476  $MC_{\text{rBC}}$  was observed in the early morning and evening, indicating the increased  
477 contribution of local traffic emissions. Despite potential large uncertainties in the  
478 estimated contribution from the local traffic to rBC, due to the many assumptions  
479 employed, its relative variation is clearly demonstrated. Further research measuring  
480 sizes of rBC directly from various sources, including coal combustion, biomass  
481 burning and traffic exhaust, is needed to validate the findings presented in this study.  
482 This work provides a relatively simple but novel method to extract the contribution of  
483 the local traffic to the rBC on the basis of the size distribution measurements of the  
484 rBC in atmosphere, which could enhance source apportionment research in urban  
485 Beijing and elsewhere where air pollution is severe.

486

#### 487 **Acknowledgments:**

488 This work was supported by the National Natural Science Foundation of China (No.  
489 91644217, 41575150 and 41305128), the Special Scientific Research Funds for  
490 Environment Protection Commonwealth Section (No. 201409027), and the Jiangsu  
491 Collaborative Innovation Center for Climate Change.

492

493 **References:**

- 494 Alexander, D. T. L., Crozier, P. A., and Anderson, J. R.: Brown carbon spheres in East Asian  
 495 outflow and their optical properties, *Sciences*, 321, 833–836, 2008.
- 496 Allen, J. O., Mayo, P. R., Hughes, L. S., Salmon, L. G., and Cass, G. R.: Emissions of  
 497 size-segregated aerosols from on-road vehicles in the Caldecott Tunnel, *Environ. Sci.*  
 498 *Technol.*, 35, 4189–4197, 2001.
- 499 Baumgardner, D., Popovicheva, O., Allan, J., Bernardoni, V., Cao, J., Cavalli, F., Cozic, J.,  
 500 Diapouli, E., Eleftheiadis, K., Genberg, P. J., Gonzalez, C., Gysel, M., John, A., Kirchstetter,  
 501 T. W., Kuhlbusch, T. A. J., Laborde, M., Lack, D., Müller, T., Niessner, R., Petzold, A.,  
 502 Piazzalunga, A., Putaud, J. P., Schwarz, J., Sheridan, P., Surramanian, R., Swietlicki, E., Valli,  
 503 G., Vecchi, R., and Viana, M.: Soot reference materials for instrument calibration and  
 504 intercomparisons: a workshop summary with recommendations, *Atmos. Meas. Tech.*, 5,  
 505 1869–1887, 2012.
- 506 Bond, T. C., and Bergstrom, R. W.: Light absorption by carbonaceous particles: an investigative  
 507 review, *Aerosol Sci. Technol.*, 40, 27–67, 2006.
- 508 Cao, J. J., Lee, S. C., Chow, J. C., Watson, J. G., Ho, K. F., Zhang, R. J., Jin, Z. D., Shen, Z. X.,  
 509 Chen, G. C., Kang, Y. M., Zou, S. C., Zhang, L. Z., Qi, S. H., Dai, M. H., Cheng, Y., and Hu,  
 510 K.: Spatial and seasonal distributions of carbonaceous aerosols over China, *J. Geophys. Res.*,  
 511 112, D22S11, doi:10.1029/2006JD008205, 2007.
- 512 Cheng, Y. F., Su, H., Rose, D., Gunthe, S. S., Berghof, M., Wehner, B., Achtert, P., Nowak, A.,  
 513 Takegawa, N., Kondo, Y., Shiraiwa, M., Gong, Y. G., Shao, M., Hu, M., Zhu, T., Zhang, Y. H.,  
 514 Carmichael, G. R., Wiedensohler, A., Andreae, M. O., and Pöschl, U.: Size-resolved  
 515 measurement of the mixing state of soot in the megacity Beijing, China: diurnal cycle, aging  
 516 and parameterization, *Atmos. Chem. Phys.*, 12, 4477–4491, 2012.
- 517 Ding, A. J., Fu, C. B., Yang, X. Q., Sun, J. N., Petäjä, T., Kerminen, V., Wang, T., Xie, Y. N.,  
 518 Herrmann, E., Zheng, L., Nie, W., Liu, Q., Wei X., and Kulmala, M.: Intense atmospheric  
 519 pollution modifies weather: a case of mixed biomass burning with fossil fuel combustion  
 520 pollution in the eastern China, *Atmos. Chem. Phys.*, 13, 10545–10554, 2013.
- 521 Ding, A. J., Huang, X., Nie, W., Sun, J. N., Kerminen, V.-M., Petäjä, T., Su, H., Cheng, Y. F., Yang,  
 522 X.-Q., Wang, M. H., Chi, X. G., Wang, J. P., Virkkula, A., Guo, W. D., Yuan, J., Wang, S. Y.,  
 523 Zhang, R. J., Wu, Y. F., Song, Y., Zhu, T., Zilitinkevich, S., Kulmala, M., and Fu, C. B.:  
 524 Enhanced haze pollution by black carbon in megacities in China, *Geophys. Res. Lett.*, 43,  
 525 2873–2879, 2016.
- 526 Gao, R. S., Schwarz, J. P., Kelly, K. K., Fahey, D. W., Watts, L. A., Thompson, T. L., Spackman, J.  
 527 R., Slowik, J. G., Cross, E. S., Han, J.-H., Davidovits, P., Onasch, T. B., and Worsnop, D. R.:  
 528 A novel method for estimating light-scattering properties of soot aerosols using a modified  
 529 single-particle soot photometer, *Aerosol Sci. Technol.*, 41, 125–135, 2007.
- 530 Gong, X. D., Zhang, C., Chen, H., Nizkorodov, S. A., Chen, J. M., and Yang, X.: Size distribution  
 531 and mixing state of black carbon particles during a heavy air pollution episode in Shanghai,  
 532 *Atmos. Chem. Phys.*, 16, 5399–5411, 2016.
- 533 Gysel, M., Laborde, M., Mensah, A., Corbin, J., Keller, A., Kim, J., Petzold, A., and Sierau, B.:  
 534 Technical note: The single particle soot photometer fails to reliably detect PALAS soot  
 535 nanoparticles, *Atmos. Meas. Tech.*, 5, 3099–3107, 2012.
- 536 Huang, X., Ding, A. J., Liu, L. X., Liu, Q., Ding, K., Niu, X. R., Nie, W., Xu, Z., Chi, X. G., Wang,

537 M. H., Sun, J. N., Guo, W. D., and Fu, C. B.: Effects of aerosol-radiation interaction on  
538 precipitation during biomass-burning season in East China, *Atmos. Chem. Phys.*, 16, 10063–  
539 10082, 2016.

540 Huang, X. F., and Yu, J. Z.: Size distributions of elemental carbon in the atmosphere of a coastal  
541 urban area in South China: characteristics, evolution processes, and implications for the  
542 mixing state, *Atmos. Chem. Phys.*, 8, 5843–5853, 2008.

543 Huang, X. F., Gao, R. S., Schwarz, J. P., He, L. Y., Fahey, D. W., Watts, L. A., McComiskey, A.,  
544 Cooper, O. R., Sun, T. L., Zeng, L. W., Hu, M., and Zhang, Y. H.: Black carbon  
545 measurements in the Pearl River Delta region of China, *J. Geophys. Res.*, 116, D12208,  
546 doi:10.1029/2010JD014933, 2011.

547 Huang, X. F., Sun, T. L., Zeng, L. W., Yu, G. H., and Luan, S. J.: Black carbon aerosol  
548 characterization in a coastal city in South China using a single particle soot photometer,  
549 *Atmos. Environ.*, 51, 21–28, 2012.

550 IPCC, 2013. Summary for policymakers. In: Stocker, T.F., Qin, D., Plattner, G.-K., Tignor, M.,  
551 Allen, S.K., Boschung, J., Nauels, A., Xia, Y., Bex, V., Midgley, P.M. (Eds.), *Climate Change*  
552 *2013: The Physical Science Basis. Contribution of Working Group I to the Fifth Assessment*  
553 *Report of the Intergovernmental Panel on Climate Change.* Cambridge University Press,  
554 Cambridge, United Kingdom and New York, NY, USA.

555 Khalizov, A. F., Xue, H. X., Wang, L., Zheng, J., and Zhang, R. Y.: Enhanced light absorption and  
556 scattering by carbon soot aerosol internally mixed with sulfuric acid, *J. Phys. Chem. A*, 113,  
557 1066–1074, 2009.

558 Kleeman, M.J., Schauer, J. J., and Cass, G. R.: Size and composition distribution of fine  
559 particulate matter emitted from motor vehicles, *Environ. Sci. Technol.* 34(7), 1132–1142,  
560 2000.

561 Laborde, M., Mertes, P., Zieger, P., Dommen, J., Baltensperger, U., and Gysel, M.: Sensitivity of  
562 the single particle soot photometer to different black carbon types, *Atmos. Meas. Tech.*, 5,  
563 1031–1043, 2012.

564 Li, J. W., and Han, Z. W.: A modeling study of severe winter haze events in Beijing and its  
565 neighboring regions, *Atmos. Res.*, 170, 87–97, 2016.

566 Liao, H., and Shang, J. J.: Regional warming by black carbon and tropospheric ozone: a review of  
567 progresses and research challenges in China, *J. Meteor. Res.*, 29, 525–545, 2015.

568 Liggio, J. Gordon, M., Smallwood, G., Li, S.-M., Stroud, C., Staebler, R., Lu, G., Lee, P., Taylor,  
569 B., and Brook, J. R.: Are emissions of black carbon from gasoline vehicles underestimated?  
570 Insights from near and on-road measurements, *Environ. Sci. Technol.*, 46, 4819–4828, 2012.

571 Lin, Y.-C., Hsu, S.-C., Chou, C.-C.-K., Zhang, R. J., Wu, Y. F., Kao, S.-J., Luo, L., Huang, C.-H.,  
572 Lin, S.-H., and Huang, Y.-T.: Wintertime haze deterioration in Beijing by industrial pollution  
573 deduced from trace metal fingerprints and enhanced health risk by heavy metals, *Environ.*  
574 *Pollut.*, 208, 284–293, 2016.

575 Liu, D., Allan, J. D., Young, D. E., Coe, H., Beddows, D., Fleming, Z. L., Flynn, M. J., Gallagher,  
576 M. W., Harrison, R. M., Lee, J., Prevot, A. S. H., Taylor, J. W., Yin, J., Williams, P. I., and  
577 Zotter, P.: Size distribution, mixing state and source apportionment of black carbon aerosol in  
578 London during wintertime, *Atmos. Chem. Phys.*, 14, 10061–10084, 2014.

579 Liu, J. W., Mo, Y. Z., Li, J., Liu, D., Shen, C. D., Ding, P., Jiang, H. Y., Cheng, Z. N., Zhang, X. J.,  
580 Tian, C. G., Chen, Y. J., and Zhang, G.: Radiocarbon-derived source apportionment of fine

581 carbonaceous aerosols before, during, and after the 2014 Asia-Pacific Economic Cooperation  
582 (APEC) summit in Beijing, China, *J. Geophys. Res. Atmos.*, 121, 4177–4187, 2016.

583 Menon, S., Hansen, J., Nazarenko, L., and Luo, Y. F.: Climate effects of black carbon aerosols in  
584 China and India, *Science*, 297, 2250–2253, 2002.

585 Moteki, N., and Kondo, Y.: Effects of mixing state on black carbon measurements by  
586 laser-induced incandescence, *Aerosol Sci. Technol.*, 41, 398–417, 2007.

587 Moteki, N., and Kondo, Y.: Method to measure time-dependent scattering cross sections of  
588 particles evaporating in a laser beam, *J. Aerosol Sci.*, 39, 348–364, 2008.

589 Peng, J. F., Hu, M., Guo, S., Du, Z. F., Zheng, J., Shang, D. J., Zamora, M. L., Zeng, L. M., Shao,  
590 M., Wu, Y.-S., Zheng, J., Wang, Y., Glen, C. R., Collins, D. R., Molina, M. J., and Zhang, R.  
591 Y.: Markedly enhanced absorption and direct radiative forcing of black carbon under polluted  
592 urban environments, *Proc. Natl. Acad. Sci. U.S.A.*, 113, 4266–4271, 2016.

593 Qin, Y., and Xie, S. D.: Spatial and temporal variation of anthropogenic black carbon emissions in  
594 China for the period 1980–2009, *Atmos. Chem. Phys.*, 12, 4825–4841, 2012.

595 Ramanathan, V., Crutzen, P. J., Kiehl, J. T., and Rosenfeld, D.: Aerosols, climate, and the  
596 hydrological cycle, *Science*, 294, 2119–2125, 2001.

597 Ramanathan, V., and Carmichael, G.: Global and regional climate changes due to black carbon,  
598 *Nature Geosci.*, 1, 221–227, 2008.

599 Schnaiter, M., Linke, C., Möhler, O., Naumann, K. H., Saathoff, H., Wagner, R., Schurath, U., and  
600 Wehner, B.: Absorption amplification of black carbon internally mixed with secondary  
601 organic aerosol, *J. Geophys. Res.*, 110, D19204, doi:10.1029/2005JD006046, 2005.

602 Schwarz, J. P., Gao, R. S., Fahey, D. W., Thomson, D. S., Watts, L. A., Wilson, J. C., Reeves, J. M.,  
603 Darbeheshti, M., Baumgardner, D. G., Kok, G. L., Chung, S. H., Schulz, M., Hendricks, J.,  
604 Lauer, A., Kärcher, B., Slowik, J. G., Rosenlof, K. H., Thompson, T. L., Langford, A. Q.,  
605 Loewenstein, M., and Aikin, K. C.: Single-particle measurements of midlatitude black carbon  
606 and light-scattering aerosols from the boundary layer to the lower stratosphere, *J. Geophys.*  
607 *Res.*, 111, D16207, doi:10.1029/2006JD007076, 2006.

608 Schwarz, J. P., Gao, R. S., Spackman, J. R., Watts, L. A., Thomson, D. S., Fahey, D. W., Ryerson,  
609 T. B., Peischl, J., Holloway, J. S., Trainer, M., Frost, G. J., Baynard, T., Lack, D. A., de Gouw,  
610 J. A., Warneke, C., and Del Negro, L. A.: Measurement of the mixing state, mass, and optical  
611 size of individual black carbon particles in urban and biomass burning emissions, *Geophys.*  
612 *Res. Lett.*, 35, L13810, doi:10.1029/2008GL033968, 2008.

613 Schwarz, J. P., Gao, R. S., Perring, A. E., Spackman, J. R., and Fahey, D. W.: Black carbon aerosol  
614 size in snow, *Sci. Rep.*, 3, 1356, doi:10.1038/srep01356, 2013.

615 Shiraiwa, M., Kondo, Y., Moteki, N., Takegawa, N., Miyazaki, Y., and Blake, D. R.: Evolution of  
616 mixing state of black carbon in polluted air from Tokyo, *Geophys. Res. Lett.*, 34, L16803,  
617 doi:10.1029/2007GL029819, 2007.

618 Shiraiwa, M., Kondo, Y., Iwamoto, T., Kita, K.: Amplification of light absorption of black carbon  
619 by organic coating, *Aerosol Sci. Technol.*, 44, 46–54, 2010.

620 Song, S., Wu, Y., Xu, J., Ohara, T., Hasegawa, S., Li, J., Yang, L., and Hao, J.: Black carbon at a  
621 roadside site in Beijing: Temporal variations and relationships with carbon monoxide and  
622 particle number size distribution, *Atmos. Environ.*, 77, 213–221, 2013.

623 Stephens, M., Turner, N., and Sandberg, J.: Particle identification by laser-induced incandescence  
624 in a solid-state laser cavity, *Appl. Opt.*, 42, 3726–3736, 2003.

625 Sun, Y. L., Jiang, Q., Wang, Z. F., Fu, P. Q., Li, J., Yang, T., and Yin, Y.: Investigation of the  
626 sources and evolution processes of severe haze pollution in Beijing in January 2013, *J.*  
627 *Geophys. Res. Atmos.*, 119, 4380–4398, 2014.

628 Wang, Q. Y., Huang, R. J., Cao, J. J., Han, Y. M., Wang, G. H., Li, G. H., Wang, Y. C., Dai, W. T.,  
629 Zhang, R. J., and Zhou, Y. Q.: Mixing state of black carbon aerosol in a heavily polluted  
630 urban area of China: implications for light absorption enhancement, *Aerosol Sci. Technol.*, 48,  
631 689–697, 2014a.

632 Wang, Q. Y., Schwarz, J. P., Cao, J. J., Gao, R. S., Fahey, D. W., Hu, T. F., Huang, R. J., Han, Y.  
633 M., and Shen, Z. X.: Black carbon aerosol characterization in a remote area of Qinghai–  
634 Tibetan Plateau, western China, *Sci. Total Environ.*, 479–480, 151–158, 2014b.

635 Wang, Q. Y., Huang, R. J., Cao, J. J., Tie, X. X., Ni, H. Y., Zhou, Y. Q., Han, Y. M., Hu, T. F., Zhu,  
636 C. S., Feng, T., Li, N., and Li, J. D.: Black carbon aerosol in winter northeastern Qinghai–  
637 Tibetan Plateau, China: the source, mixing state and optical property, *Atmos. Chem. Phys.*,  
638 15, 13059–13069, 2015a.

639 Wang, Q. Y., Liu, S. X., Zhou, Y. Q., Cao, J. J., Han, Y. M., Ni, H. Y., Zhang, N. N., and Huang, R.  
640 J.: Characteristics of Black Carbon Aerosol during the Chinese Lunar Year and Weekdays in  
641 Xi’an, China, *Atmosphere*, 6, 195–208, 2015b.

642 Wang, Q. Y., Huang, R. J., Zhao, Z. Z., Cao, J. J., Ni, H. Y., Tie, X. X., Zhao, S. Y., Su, X. L., Han,  
643 Y. M., Shen, Z. X., Wang, Y. C., Zhang, N. N., Zhou, Y. Q., and Corbin, J. C.:  
644 Physicochemical characteristics of black carbon aerosol and its radiative impact in a polluted  
645 urban area of China, *J. Geophys. Res. Atmos.*, 121, doi:10.1002/2016JD024748, 2016.

646 Wang, Y., Khalizov, A., Levy, M., and Zhang, R. Y.: New direction: light absorbing aerosols and  
647 their atmospheric impacts, *Atmos. Environ.*, 81, 713–715, 2013.

648 Wang, Y. Q., Zhang, X. Y., and Arimoto, R.: The contribution from distant dust sources to the  
649 atmospheric particulate matter loadings at Xi’an, China during spring, *Sci. Total Environ.*,  
650 368, 875–883, 2006.

651 Wang, Y. Q., Zhang, X. Y., and Draxler, R. R.: TrajStat: GIS-based software that uses various  
652 trajectory statistical analysis methods to identify potential sources from long-term air  
653 pollution measurement data, *Environ. Modell. Softw.*, 24, 938–939, 2009.

654 Wu, Y. F., Zhang, R. J., Tian, P., Tao, J., Hsu, S.-C., Yan, P., Wang, Q. Y., Cao, J. J., Zhang, X. L.,  
655 and Xia, X. A.: Effect of ambient humidity on the light absorption amplification of black  
656 carbon in Beijing during January 2013, *Atmos. Environ.*, 124, 217–223, 2016.

657 Yin, Z. C., and Wang, H. J.: Seasonal prediction of winter haze days in the north central North  
658 China Plain, *Atmos. Chem. Phys.*, 16, 14843–14852, 2016.

659 Yu, H., and Yu, J. Z.: Modal characteristics of elemental and organic carbon in an urban location  
660 in Guangzhou, China, *Aerosol Sci. Technol.*, 43, 1108–1118, 2009.

661 Yu, H., Wu, C., Wu, D., and Yu, J. Z.: Size distributions of elemental carbon and its contribution to  
662 light extinction in urban and rural locations in the Pearl River Delta region, China, *Atmos.*  
663 *Chem. Phys.*, 10, 5107–5119, 2010.

664 Zhang, Q., Quan, J. N., Tie, X. X., Li, X., Liu, Q., Gao, Y., and Zhao, D. L.: Effects of  
665 meteorology and secondary particle formation on visibility during heavy haze events in  
666 Beijing, China, *Sci. Total Environ.*, 502, 578–584, 2015.

667 Zhang, R., Jing, J., Tao, J., Hsu, S.-C., Wang, G., Cao, J., Lee, C.S.L., Zhu, L., Chen, Z., Zhao, Y.,  
668 and Shen, Z.: Chemical characterization and source apportionment of PM<sub>2.5</sub> in Beijing:



669 seasonal perspective, *Atmos. Chem. Phys.*, 13, 7053–7074, 2013.

670 Zhang, R. Y., Khalizov, A. F., Pagels, J. Zhang, D., Xue, H. X., and McMurry, P. H.: Variability in  
671 morphology, hygroscopicity, and optical properties of soot aerosols during atmospheric  
672 processing, *Proc. Natl. Acad. Sci. U.S.A.*, 105, 10291–10296, 2008a.

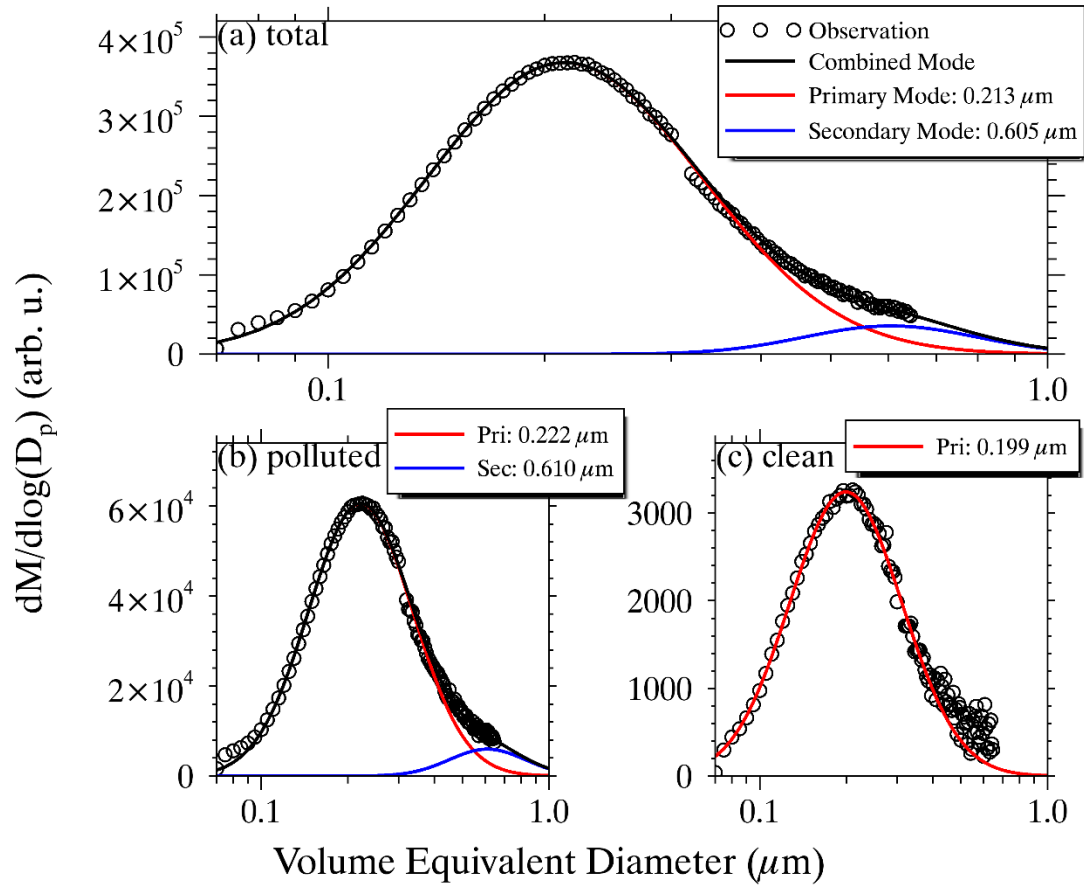
673 Zhang, X. Y., Wang, Y. Q., Zhang, X., Guo, W., and Gong, S. L.: Carbonaceous aerosol  
674 composition over various regions of China during 2006, *J. Geophys. Res.*, 113, D14111,  
675 doi:10.1029/2007JD009525, 2008b.

676 Zhang, Y.-L., Huang, R.-J., El Haddad, I., Ho, K.-F., Cao, J.-J., Han, Y., Zotter, P., Bozzetti, C.,  
677 Daellenbach, K. R., Canonaco, F., Slowik, J. G., Salazar, G., Schwikowski, M.,  
678 Schnelle-Kreis, J., Abbaszade, G., Zimmermann, R., Baltensperger, U., Prévôt, A. S. H., and  
679 Szidat, S.: Fossil vs. non-fossil sources of fine carbonaceous aerosols in four Chinese cities  
680 during the extreme winter haze episode of 2013, *Atmos. Chem. Phys.*, 15, 1299–1312, 2015.

681 Zheng, G. J., Duan, F. K., Su, H., Ma, Y. L., Cheng, Y., Zheng, B., Zhang, Q., Huang, T., Kimoto,  
682 T., Chang, D., Pöschl, U., Cheng, Y. F., and He, K. B.: Exploring the severe winter haze in  
683 Beijing: the impact of synoptic weather, regional transport and heterogeneous reactions,  
684 *Atmos. Chem. Phys.*, 15, 2969–2983, 2015.

685

686



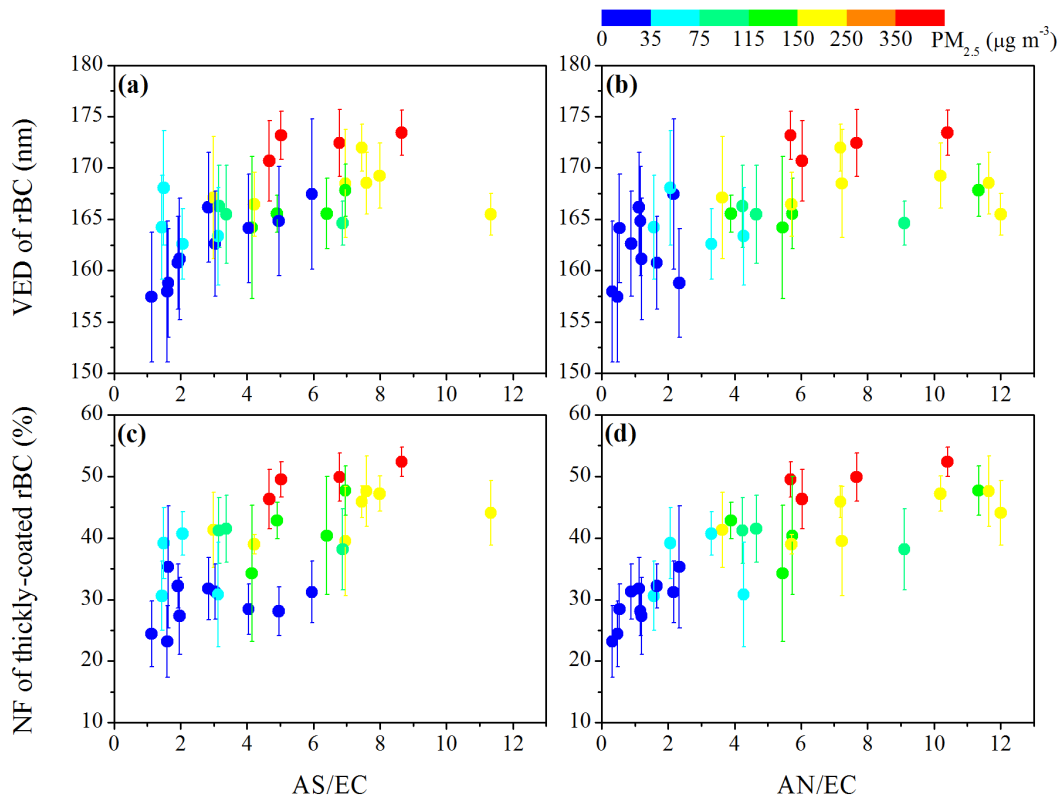
687

688 Fig. 1. Size distributions of rBC in volume-equivalent diameter during a campaign from 24

689 February to 15 March, 2014. The red and blue lines are the lognormal fittings to the primary and

690 secondary modes, respectively, and the black ones correspond to the combined mode.

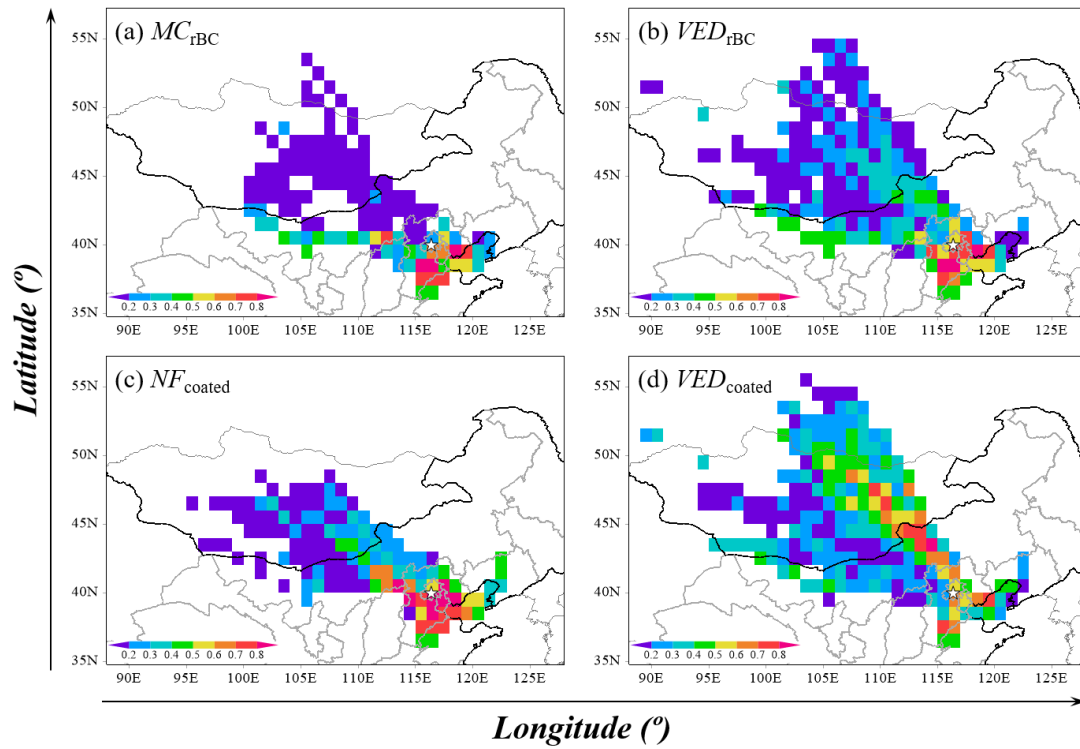
691



692

693 Fig. 2. Variation in the average volume-equivalent diameters of rBC ( $VED_{rBC}$ ) as a function of the  
 694 mass ratios of (a) ammonium sulfate (AS) and (b) ammonium nitrite (AN) to elemental carbon  
 695 (EC). The same apply for (c) and (d), but for the number fraction of thickly coated rBC ( $NF_{coated}$ ).  
 696 The vertical bar denotes one standard deviation. The color scale represents the pollution levels  
 697 defined as the  $PM_{2.5}$  mass concentration according to the AQI standard of MEP of China.

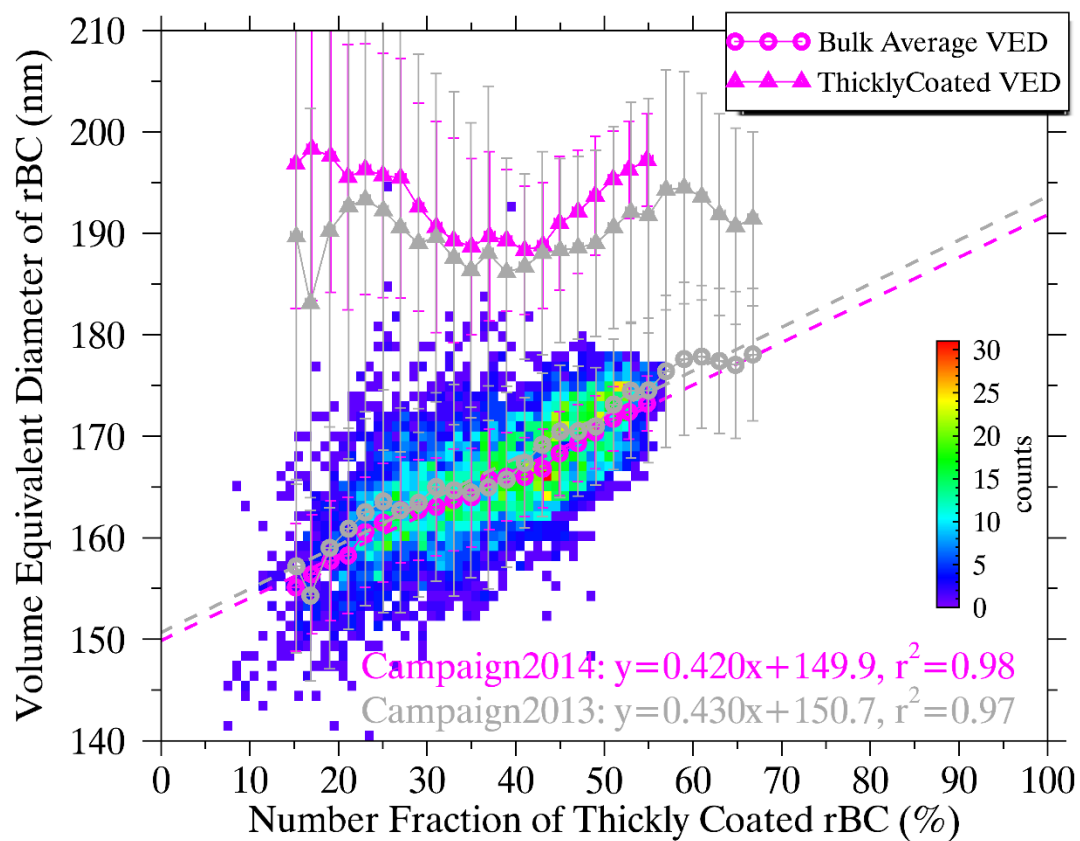
698



699

700 Fig. 3. Distributions of gridded ( $1^\circ \times 1^\circ$ ) potential source contribution functions of (a) mass  
 701 concentration ( $MC$ ) and (b) volume equivalent diameter ( $VED$ ) of rBC, and (c) number fraction  
 702 ( $NF$ ) and (d)  $VED$  of thickly coated rBC. The overlaid star symbol represents the geographical  
 703 location of the observation site.

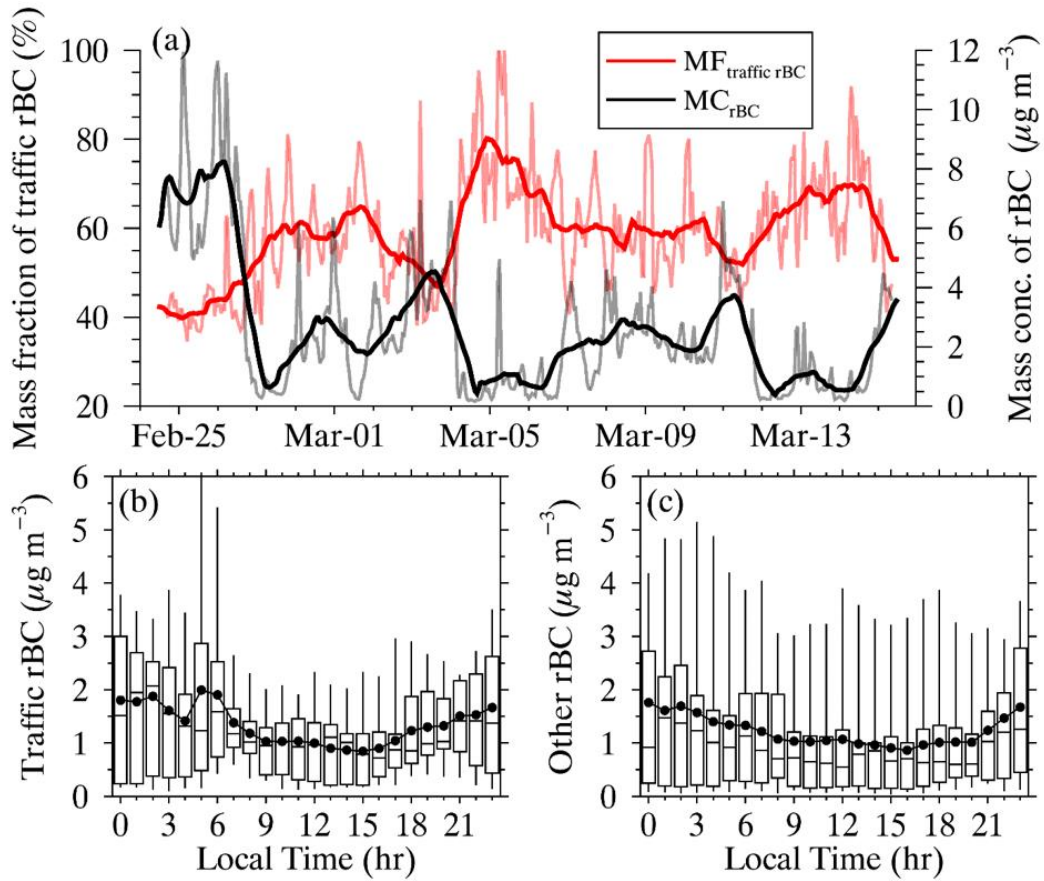
704



705

706 Fig. 4. Two-dimensional histogram of the 5-min average volume equivalent diameter of rBC  
 707 ( $VED_{rBC}$ ) against number fraction of thickly coated rBC ( $NF_{coated}$ ) during the campaign in the late  
 708 winter in 2014. The magenta circles and triangles with error bars represent the mean  $VED_{rBC}$  and  
 709  $VED$  of thickly-coated rBC ( $VED_{coated}$ ) averaged in each  $NF_{coated}$  bin with a resolution of 2%,  
 710 respectively. The dashed magenta line denotes the linear regression of  $VED_{rBC}$  against  $NF_{coated}$ .  
 711 The relationship between  $VED_{rBC}$  and  $NF_{coated}$  during another campaign in January 2013 (Wu et al.,  
 712 2016) is comparatively overlapped in gray.

713



714

715 Fig. 5. (a) Time series of hourly mass concentration of rBC ( $MC_{\text{rBC}}$ ) and mass fraction of local  
 716 traffic related rBC ( $MF_{\text{traffic}}$ ). The bold lines represent the variations of the daily moving averaged  
 717  $MC_{\text{rBC}}$  and  $MF_{\text{traffic}}$ . (b) and (c) show the diurnal variations in the decomposed rBC from local  
 718 traffic emission and other sources, respectively.